

# Highly ordered graphene architectures by duplicating melamine sponges as a three-dimensional deformation-tolerant electrode

Le Li, Kai Wang, Zhaoqi Huang, Chao Zhang (✉), and Tianxi Liu (✉)

State Key Laboratory for Modification of Chemical Fibers and Polymer Materials & College of Materials Science and Engineering, Donghua University, Shanghai 201620, China

**Received:** 26 April 2016

**Revised:** 12 June 2016

**Accepted:** 13 June 2016

© Tsinghua University Press and Springer-Verlag Berlin Heidelberg 2016

## KEYWORDS

graphene, layer-by-layer self-assembly, highly ordered architecture, conducting polymer, deformation-tolerant electrode

## ABSTRACT

In this study, macroscopic graphene-wrapped melamine foams (MF-G) were fabricated by an MF-templated layer-by-layer (LBL) assembly using graphene oxide as building blocks, followed by solution-processed reduction. By concisely duplicating sponge-like, highly ordered three-dimensional architectures from MF, the resulting MF-G with an interconnected graphene-based scaffold and tunable nanostructure was explored as compressible, robust electrodes for efficient energy storage. A thin layer of pseudocapacitive polypyrrole (PPy) was then attached and uniformly coated on MF-G, resulting in a well-defined core-double-shell configuration of the MF-G-PPy ternary composite sponges. The as-assembled devices exhibited enhancement of supercapacitor performance, with a high specific capacitance of  $427 \text{ F}\cdot\text{g}^{-1}$  under a compressive strain of 75% and an excellent cycling stability with only 18% degradation after 5,000 charge-discharge cycles. Besides, the MF-G-PPy electrode maintained stable capacitance up to 100 compression-release cycles, with a compressive strain of 75%. These encouraging results thus provide a new route towards the low-cost, easily scalable fabrication of lightweight and deformation-tolerant electrodes.

## 1 Introduction

In recent years, supercapacitors, which are also referred to as electrochemical capacitors or ultracapacitors, have attracted tremendous attention, attributed to their high powder density, relatively high energy density, and long cycling life [1–6]; supercapacitors can store and deliver a large amount of charge in a short

period of time; as a result, they exhibit a power density greater than that of batteries, and bridge the gap between conventional capacitors and batteries [7–10]. As compared with conventional supercapacitors, flexible supercapacitors with a lightweight, bendable feature demonstrate significant promise for wearable electronics, attributed to an increasing demand for sustainable energy in the future [11–18].

Address correspondence to Chao Zhang, czhang@dhu.edu.cn; Tianxi Liu, txliu@fudan.edu.cn

Beyond the efforts focused particularly on the development of flexible supercapacitor systems with a bendable performance [11, 19–24], however, few attempts have been devoted to the achievement of flexible supercapacitors exhibiting deformation-tolerant abilities [25–27]. Particularly, a class of foam-like, porous materials with three-dimensional (3D) interconnected architectures are necessary for fabricating such compressive electrodes for meeting the various requirements of modern power portable equipment [27–32]. These electrode materials can be classified into two types: (1) carbon foams, which are typically prepared by the pyrolysis of polymer foams with high porosities [33–36]; (2) carbon nanotubes (CNTs) or graphene-based macroform, such as CNT/graphene foams and graphene aerogels [37–41]. However, it is particularly difficult to synthesize such 3D foam-like carbon structures with strong robustness, which easily tend to collapse or distort under compression, attributed to their inherent poor compressibility and springiness [32, 42, 43]. Meanwhile, it is always challenging to meet the large-scale production demand for developing such 3D foam-like carbon structures, which are typically prepared by a high-cost, complex synthesis process. Hence, the key challenge in developing deformation-tolerant supercapacitors is the manner of selecting and fabricating highly compressive electrode materials with high capacity and excellent mechanical stability [44–48].

Graphene, a two-dimensional monolayer of a  $sp^2$ -carbon network, has been widely used as a promising electrode material, attributed to its excellent electrical conductivity, high surface area, and easily tunable structure and property [17]. However, graphene sheets are prone to strong aggregation, thereby resulting in the decrease of the surface area, and consequently the capacitive performance of the resulting graphene. On the other hand, commercial polymer foams, such as melamine foams (MFs), with an extremely low density ranging from 4 to 12  $\text{mg}\cdot\text{cm}^{-3}$  and an ultrahigh porosity greater than 99% are ideal candidates as substrates for the large-scale production of compressible electrode materials [33]. However, few studies have reported flexible electrode materials based on polymer foam with highly deformation-tolerant ability [46].

In this study, we propose a rational design and

assembly of a lightweight, low-cost, and deformation-tolerant 3D electrode material, which consists of a commercial MF core and nanostructured graphene/polypyrrole (PPy) double shells (MF-G-PPy). The ternary MF-G-PPy composite sponges with a core-double-shell skeleton completely exploit superelasticity and high conductivity provided by MFs and graphene, respectively. Enhancement in the electrochemical performance of the MF-G-PPy electrode is observed, which benefits from a synergistic effect via the combination of graphene and PPy with a tailored nanostructure. Thus, this core-double-shell sponge facilitates a possible, efficient route for the fabrication of a high-performance electrode with a predefined configuration and precise control.

## 2 Experimental

### 2.1 Materials

MF obtained from SINOYQX (Sichuan, China) was used as received. Natural graphite powder (325 mesh) was purchased from Alfa Aesar. A polyethylene imine (PEI) solution ( $M_w = 70,000$ , 50 wt.% in water) was obtained from Aladdin Chemical Reagent. Pyrrole was purchased from Sigma-Aldrich and distilled before use. All other reagents purchased from Sinopharm Chemical Reagent Co. Ltd. were used without further purification. Deionized (DI) water was used throughout the experiments.

### 2.2 Preparation of MF-G

MF-G was prepared by the layer-by-layer (LBL) assembly method based on electrostatic interactions of positively charged PEI and negatively charged graphene oxide (GO) sheets. A 1  $\text{mg}\cdot\text{mL}^{-1}$  PEI solution was prepared by diluting a 50 wt.% PEI solution using DI water. GO was prepared according to a modified Hummers method [49]. The synthesized GO powder was suspended and ultrasonicated in DI water, affording a colloidal suspension of GO with a concentration of 1.0  $\text{mg}\cdot\text{mL}^{-1}$ . Then, LBL fabrication was carried out by alternately immersing the MFs into a cationic (PEI) solution and an anionic (GO) suspension for 1 min and removing the excess adsorbed material (PEI and GO) by rinsing several times with DI water.

The content of GO assembled on the skeleton surface of MF was precisely controlled by changing the number of bilayers. MF-GO was successively treated further with hydrazine hydrate (85%) at 90 °C for 1 h, furnishing MF-G. Upon reduction, MF-G was washed with excess DI water and dried in a vacuum oven at 50 °C.

### 2.3 Preparation of MF-G-PPy

MF-G-PPy was prepared by the *in situ* polymerization of pyrrole on the MF-G template. Polymerization was conducted in an ice-water bath at ~0 °C. Typically, a piece of MF-G was first immersed into a 50 mL aqueous solution with a designed amount of pyrrole. Second, another 50 mL aqueous solution of ammonium persulfate (APS) was added, with the molar ratio of pyrrole to APS was 1:1. Next, after polymerization for 12 h, the sponge was removed and washed several times with DI water, followed by drying overnight under vacuum at 50 °C. Hereafter, the resultant PPy-coated MF-G sponges are referred to as MF-G-PPy-1, MF-G-PPy-2, and MF-G-PPy-3, respectively, corresponding to a series of MF-G-PPy containing different initial pyrrole concentrations of 0.01, 0.03, and 0.05 M, respectively. The content of PPy in MF-G-PPy was calculated from the mass changes of sponges before and after polymerization.

### 2.4 Characterization

Field-emission scanning electron microscopy (FESEM, Ultra 55, Zeiss) was employed to observe the morphology of the sponge samples. Raman spectra were recorded on a Dilor LABRAM-1B multi-channel confocal microspectrometer with a laser excitation of 631 nm. Stress–strain measurements of the sponge samples were conducted using an Instron Universal Testing Machine (model 5567). The maximum compression strain ( $\epsilon$ ) was set to 0.8, and the compression-releasing speed was 0.1 cm·s<sup>-1</sup>.

### 2.5 Electrochemical measurements

Symmetric supercapacitor cells were fabricated using two pieces of MF-G-PPy samples having the same weight, separated by a filter paper. The as-fabricated two-electrode device was immersed into a 1 M

potassium chloride (KCl) electrolyte. Cyclic voltammetry (CV) and galvanostatic charge–discharge profiles were recorded on a CHI 660D electrochemical workstation (CHI Instruments). The specific capacitance of the supercapacitor device was calculated from the CV curves according to Eq. (1):

$$C = \int \frac{I}{m} dV / v \Delta V \quad (1)$$

where  $I$  is the response current (A),  $m$  is the total mass of active materials, such as graphene and PPy on the two electrodes (g),  $\Delta V$  is the potential range (V), and  $v$  is the potential scan rate (V·s<sup>-1</sup>). AC impedance measurements were conducted from 0.01 to 10<sup>6</sup> Hz with an AC amplitude of 5 mV.

## 3 Results and discussion

The LBL assembly of MF-G using commercial MFs as template is illustrated in Fig. 1. The bare MFs were covered with LBL GO/PEI coatings by the alternate adsorption of anionic GO sheets and cationic PEI by employing a conventional electrostatic LBL assembly technique [50–52]. MFs exhibited an open-cell microstructure, which is convenient for the infiltration of a polyelectrolyte-containing solution. By soaking in a 10% hydrazine hydrate solution at 90 °C, electroconductive chemically reduced graphene layers were obtained on the MF skeleton. The  $\pi$ -conjugation network within graphene sheets was gradually recovered during reduction, as evidenced by the Raman spectra of MF-GO before and after reduction (Fig. S1 in the Electronic Supplementary Material (ESM)). Two intensive bands were observed at 1,582 and 1,358 cm<sup>-1</sup>, respectively, in the Raman spectra of MF-GO and MF-G; these values corresponded to the characteristic D and G bands, respectively. For MF-G, the  $I_D/I_G$  ratio (1.20) increased as compared to that observed for MF-GO (1.03), indicating that the average size of the sp<sup>2</sup> domains decreases by the reduction of exfoliated GO, along with the formation of more numerous new graphitic domains. Upon reduction, highly controllable graphene layers in terms of thickness can be achieved by the simple construction of different numbers of LBL bilayers on MFs.

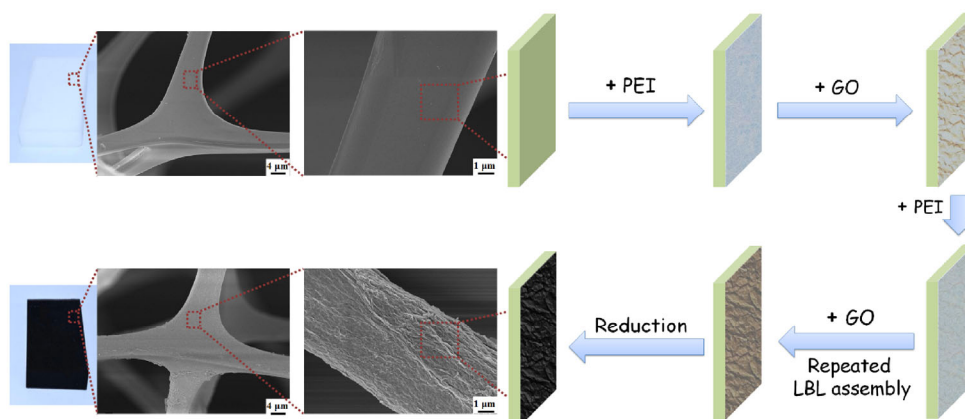


**Figure 1** Schematic of the fabrication of MF-G sponge by MFs via LBL assembly.

For monitoring the LBL deposition of graphene layers on the MF skeleton, four representative samples with different numbers of bilayers were chosen, hereafter denoted as MF-G-4 (4 bilayers), MF-G-6 (6 bilayers), MF-G-8 (8 bilayers), and MF-G-10 (10 bilayers), for observing the morphology evolution of MFs after LBL deposition (Fig. 2). Bare MFs exhibited a smooth skeleton surface (Figs. 2(a) and 2(b)), while homogenous coatings were observed in the MF-G samples up to 8 bilayers (Figs. 2(g) and 2(h)). These thin graphene coatings were observed around the cell walls, which duplicate the complex geometry of the 3D intercrossed MF skeleton, and did not alter the unique open-cell microstructure. With the addition of increasing number of bilayers, the MF-G skeleton exhibited a rougher surface with a wrinkled appearance

(Figs. 2(c)–2(h)). The loading of graphene deposited on MFs was determined to be 2.01 wt.% (MF-G-4), 2.32 wt.% (MF-G-6), and 2.48 wt.% (MF-G-8). For the MF-G-10 sample (Fig. S2 in the ESM), excess graphene layers partially blocked the pores of the MFs, thereby damaging the open-cell microstructure. This assembly process for constructing graphene into a 3D interconnected framework is completely different from other methods, such as the synthesis of 3D graphene on nickel foams under optimal conditions of chemical vapor deposition (CVD). Different from the CVD growth of 3D graphene, which depends on the size of nickel foams, the LBL assembly method utilizes commercial polymer foams that are easily produced in any shape and size; this characteristic is beneficial for fabricating extremely large-sized 3D graphene

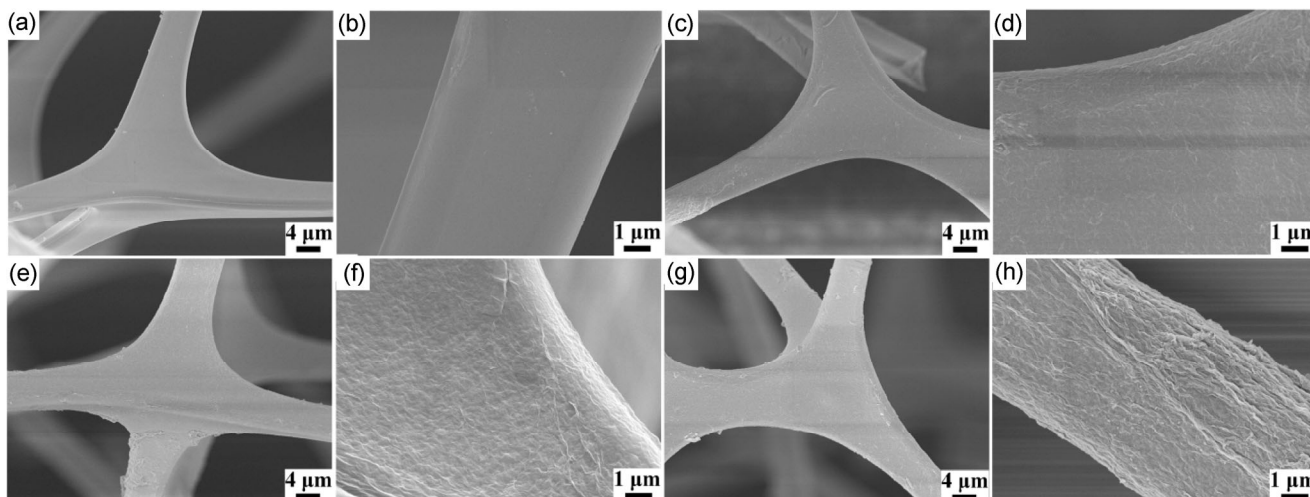


**Figure 2** Low- and high-magnification SEM images of ((a) and (b)) bare MFs, ((c) and (d)) MF-G-4, ((e) and (f)) MF-G-6, and ((g) and (h)) MF-G-8, respectively.

frameworks.

Next, a pseudocapacitive material, PPy, was introduced to wrap the 3D porous graphene network via *in situ* polymerization, forming a ternary MF-G-PPy composite sponge. As a result, a synergistic effect leading to the enhancement of supercapacitor performance is expected [31]. The thickness of the PPy layers can be easily controlled by varying the initial pyrrole concentration. The loading of PPy deposited on MF-G-6 was determined to be 3.18 wt.% (MF-G-PPy-1), 3.92 wt.% (MF-G-PPy-2), and 6.23 wt.% (MF-G-PPy-3). As shown in Fig. 3, different from the wrinkled surface of MF-G samples, attributed to the coating of graphene on the MF skeleton, relatively rough surface with a spot of PPy particles was obtained by the immobilization of PPy on graphene. The increase of the initial pyrrole concentration resulted in more aggregation of PPy particles on the surface. As shown in Fig. 3(g), the cross-sectional SEM image of MF-G-PPy-2 clearly indicated the presence of two alternating layers (graphene and PPy layers in sequence) with a total thickness of  $\sim 250$  nm (denoted by red arrows) on the MF cell wall. As shown in Fig. 3(h), the MF-G-PPy-2 sample exhibited a similar morphology after tensile failure, and the closely compacted edges of the graphene and PPy layers clearly indicated strong adhesion without the introduction of any void or defects between each layer. Interaction was observed between the basal plane of the graphene surface and

the aromatic structure of PPy through  $\pi$ - $\pi$  stacking, which promotes the strong adhesion of graphene and PPy layers.

For fabricating lightweight, deformation-tolerant electrodes, commercial MFs were used as templates and substrates for the sequential immobilization of graphene and PPy layers. The key factor in determining the final supercapacitor performance is to exploit the optimized thickness of a graphene layer combined with an appropriate PPy loading, affording a 3D composite electrode. CV and chronopotentiometry (CP) were employed for characterizing the electrochemical performance of the resulting MF-G-PPy composite in a typical two-electrode system. Figure 4(a) shows the CV curves of the MF-G-PPy-1, MF-G-PPy-2, and MF-G-PPy-3 composites at a scan rate of  $10 \text{ mV}\cdot\text{s}^{-1}$ . With increasing loading of PPy, the specific capacitance of the MF-G-PPy-2 electrode increased to an optimized value of  $411 \text{ F}\cdot\text{g}^{-1}$ . With increasing thickness of the PPy layer, charge transport length, as well as the diffusion resistance of electrolyte ions, increased during charge–discharge, resulting in the weakened electrochemical performance of the MF-G-PPy-3 electrode. Besides, the effect of the thickness of graphene layers within the MF-G sponges on the electrochemical performance was also investigated for optimizing the resulting performance (Fig. S3 in the ESM). MF-G-PPy-2 with six GO/PEI bilayers and a pyrrole concentration of 0.03 M exhibited an

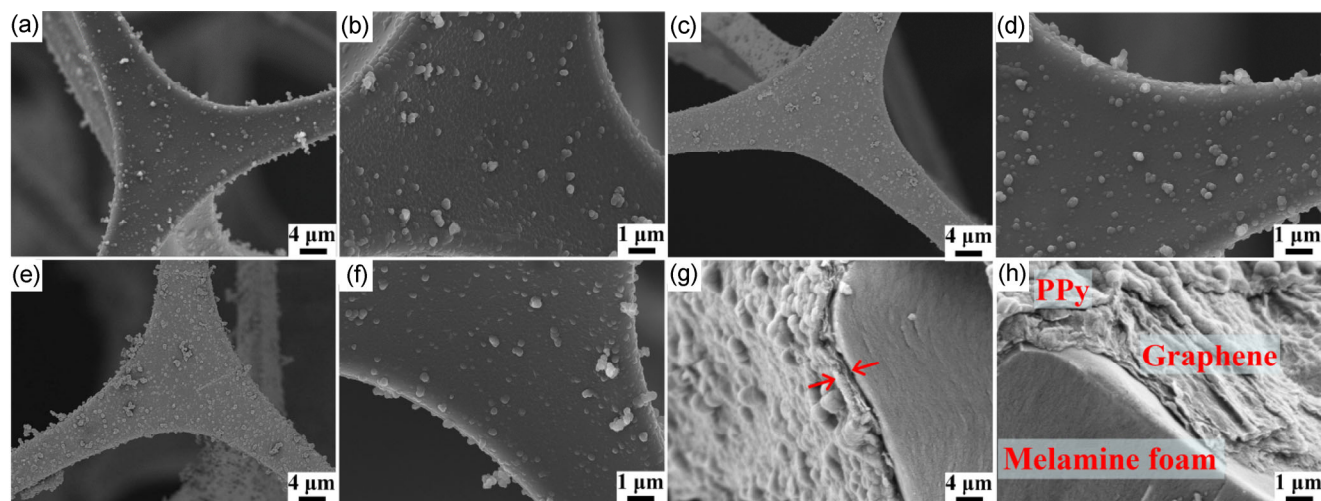


**Figure 3** Low- and high-magnification SEM images of ((a) and (b)) MF-G-PPy-1, ((c) and (d)) MF-G-PPy-2, and ((e) and (f)) MF-G-PPy-3, respectively. Cross-sectional SEM images of fractured MF-G-PPy-2 samples (g) before and (h) after tensile failure.

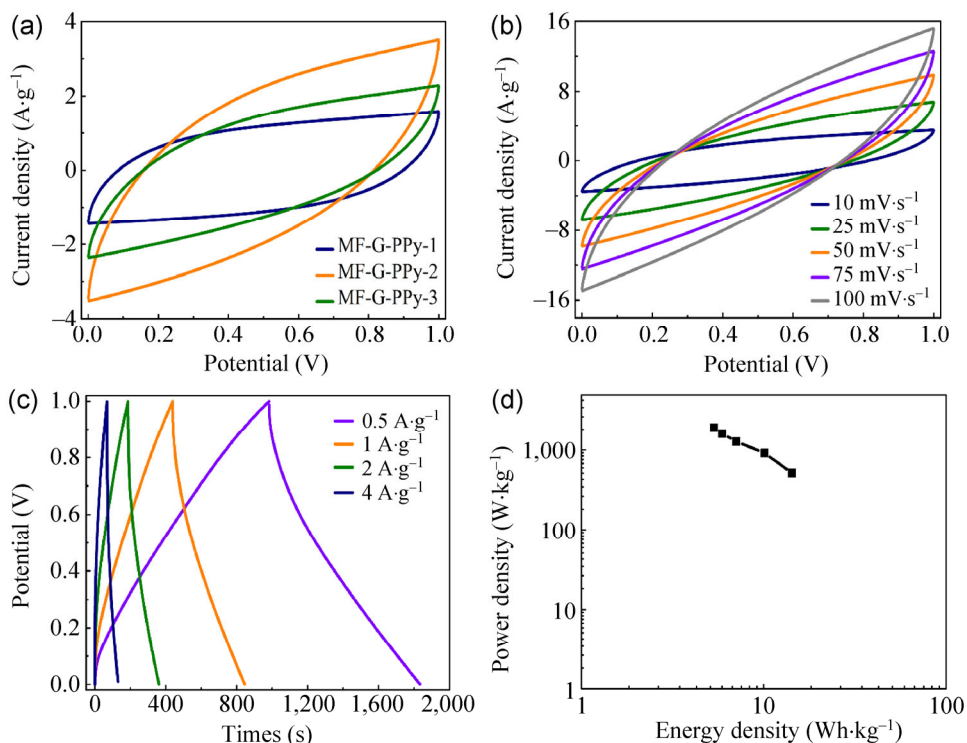


**Figure 4** (a) CV curves of MF-G-PPy-1, MF-G-PPy-2, and MF-G-PPy-3 at a scan rate of  $10 \text{ mV}\cdot\text{s}^{-1}$ . (b) CV curves of MF-G-PPy-2 at various scan rates from 10 to  $100 \text{ mV}\cdot\text{s}^{-1}$ . (c) Galvanostatic charge/discharge curves of MF-G-PPy-2 at various current densities from 0.5 to  $4 \text{ A}\cdot\text{g}^{-1}$ . (d) Ragone plots of as-fabricated deformation-tolerant supercapacitor devices.

optimized electrochemical performance. As shown in Fig. 4(b), MF-G-PPy-2 exhibited rectangular CV curves, indicative of ideal capacitive behavior; this observation implies that ions diffused from the electrolyte can easily access the active electrode material. With increasing scan rates, the redox current density of the MF-G-PPy-2 electrode simultaneously increased, indicating rapid ion exchange during charge–discharge. Considering CV curves with an almost rectangular shape, a relatively high specific capacitance of  $411 \text{ F}\cdot\text{g}^{-1}$  was obtained for the electrodes at a scan rate of  $10 \text{ mV}\cdot\text{s}^{-1}$ . The favorable capacitive behavior is attributed to the rapid diffusion and easy transport of electrolyte ions through the highly porous network, and a highly conductive graphene network facilitates a fast transport of electrons during the charge–discharge process. Meanwhile, at different densities, the MF-G-PPy-2 electrode (Fig. 4(c)) exhibited nearly triangular CP curves, without any distinct plateau region. This phenomenon further confirms that rapid ion exchange and electron transport occur during charge–discharge. Specific capacitance and Coulombic

efficiencies at various current densities were also calculated from the CP curves. For the MF-G-PPy-2 electrode, the calculated specific capacitance was  $427 \text{ F}\cdot\text{g}^{-1}$  at a current density of  $0.5 \text{ A}\cdot\text{g}^{-1}$ . Although the specific capacitance gradually decreased with increasing current density as insufficient active material is involved in the redox reaction at high current densities, the specific capacitance of the MF-G-PPy-2 electrode still reached  $249 \text{ F}\cdot\text{g}^{-1}$  at  $4 \text{ A}\cdot\text{g}^{-1}$ , maintaining a retention of approximately 58% at a high current density. Furthermore, even at a low current density, from the CP curves, the Coulombic efficiencies for MF-G-PPy-2 maintained a relative high value (greater than 90%). Figure 4(d) shows a representative Ragone plot calculated for the as-fabricated deformation-tolerant supercapacitor device, and the maximum energy density and power density were  $14.3 \text{ Wh}\cdot\text{kg}^{-1}$  and  $2.0 \text{ kW}\cdot\text{kg}^{-1}$ , respectively.

Based on the superior compression performance of MFs, the resulting MF-G-PPy electrodes are expected to exhibit excellent deformation-tolerant performance. Figure 5(a) shows the compression–release of the

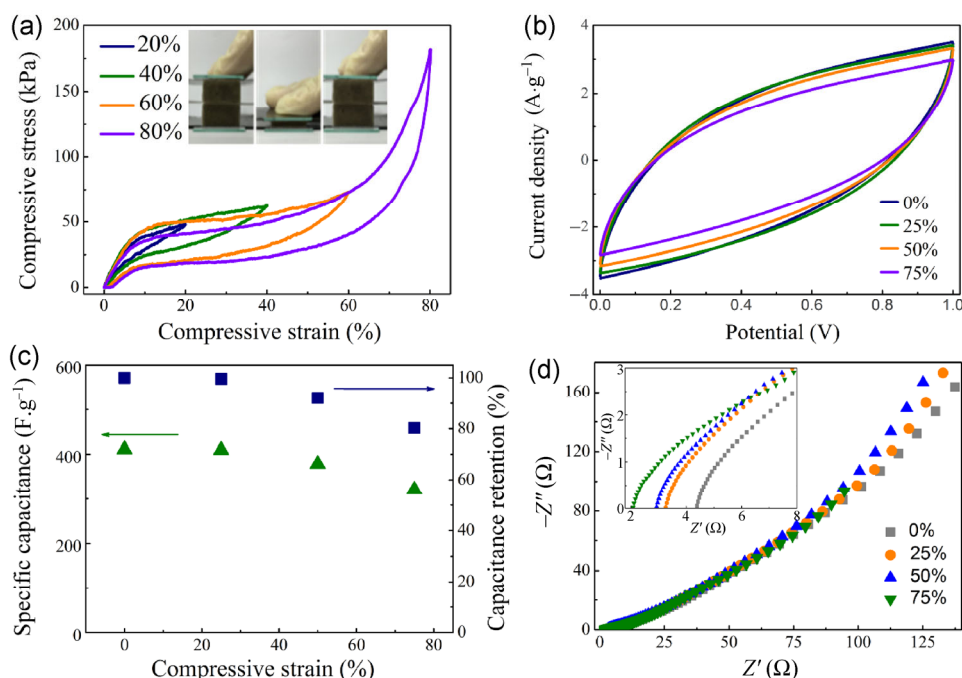


**Figure 5** (a) Stress–strain curves of the MF-G-PPy-2 electrode at different strains of 20%, 40%, 60%, and 80%. An optical image of an assembled supercapacitor device demonstrating compression and recovery. (b) CV curves of the MF-G-PPy-2 electrode under different compressive strain from 0% to 75% at a scan rate of  $10 \text{ mV}\cdot\text{s}^{-1}$ . (c) Specific capacitance and capacitance retention of the MF-G-PPy-2 electrode at different compressive strain. (d) Nyquist plots of the MF-G-PPy-2 electrode at different compressive strain. Inset shows the magnification of the high-frequency region from the spectra.

as-fabricated supercapacitor device. The compressive stress–strain behavior of the resultant MF-G-PPy electrode is a factor indicative of an open-cell structure, namely, elastic behavior at low strain, cell-collapse-related stress reduction at intermediate strain, and plastic stiffening at high strain. Because the MFs exhibited a robust structure and strong adhesion was observed between graphene and PPy layers, compression stress reached a maximum of greater than 180 kPa, the value of which is superior to that of other 3D compressible electrode materials to the best of our knowledge (Table S1 in the ESM) [28, 31, 33, 46]. The inset in Fig. 5(a) shows the compression–release process; the device returned to its original shape without plastic deformation. CV tests were (Fig. 5(b)) performed for investigating the electrochemical behavior of the MF-G-PPy-2 electrode withstanding different compression ratios, and Fig. 5(c) shows the specific capacitances. The MF-G-PPy-2 electrode exhibited similar CV curves, with marginal changes in capacitive performance under 25% and 50% compressive strain as compared to the original state (0%). The specific

capacitance retention withstanding a compressive strain of 50% was retained at 92.1%. Such superior compression-tolerant performance has rarely been reported for supercapacitors (Table S1 in the ESM) [28, 31, 33, 46]. For investigating the ultimate performance of the 3D sponge electrode tolerating compression, the MF-G-PPy-2 electrode was further compressed at a strain of 75%. At such a high compressive strain, several other compressive electrodes, such as carbon foams and graphene aerogels, lose their elasticity and even collapse without recovery. However, the CV curve of the MF-G-PPy-2 electrode withstanding a compressive strain of 75% only exhibited a slight decrease; this retention of capacitance was maintained at 80.3% at such a high compressive strain, attributed to the unique 3D open-cell network of the MF-G-PPy-2 electrode; this network is extremely critical for rapid ion diffusion and electron transport. Electrochemical impedance spectroscopy (EIS) is an electrochemical method effective for probing the features of electrodes, such as microstructure, conductivity, and charge transport at the interface between

the electrode and electrolyte. Figure 5(d) shows the Nyquist plots for the MF-G-PPy-2 electrode at frequencies ranging from  $10^6$  to 0.01 Hz at different compressive strain values from 0% to 75%. The inset of Fig. 5(d) shows the high-frequency region of EIS curves. The Nyquist plots of the MF-G-PPy-2 electrode withstanding different compressive strain exhibited almost the same behavior at different frequency ranges. At the beginning of the Nyquist plots, the intercept for the real component ( $R_s$ ) represents the solution and internal resistances of the electrode material. Under different compressive strain values, the  $R_s$  values of the MF-G-PPy-2 electrode were less than  $5 \Omega$ . With increasing compressive strain,  $R_s$  decreased, attributed to better contact between the electrode and current collector. At a low-frequency region, all EIS curves exhibited a straight, nearly vertical line, indicating ideal capacitive behavior and typical ion diffusion in the 3D porous framework of sponge electrodes. Combined with the excellent mechanical properties of the resultant 3D electrodes listed above, the high

performance of such electrodes provides an efficient route for fabricating new deformation-tolerant supercapacitors on a large scale. In addition, the high deformation-tolerant performance of the resultant devices may accommodate stresses related to the volume expansion of conducting polymers during charge–discharge cycles.

The cycling stability of electrode materials is another critical parameter that should be focused on for practical applications [20, 50]. Cycling stability tests were conducted for the MF-G-PPy-2 electrode at a scan rate of  $10 \text{ mV}\cdot\text{s}^{-1}$  under a compressive strain of 75%. As shown in Fig. 6(a), after 5,000 charge–discharge cycles, the CV curves for the MF-G-PPy-2 electrode exhibited a slight decrease in the area. For the MF-G-PPy-2 electrode, the specific capacitance decreased from 330 to  $271 \text{ F}\cdot\text{g}^{-1}$  under a compressive strain of 75%, i.e., 82% of its initial capacitance was maintained (Fig. 6(b)). Even at a high compression state, the as-fabricated electrode with a 3D interconnected porous structure was extremely stable after long time

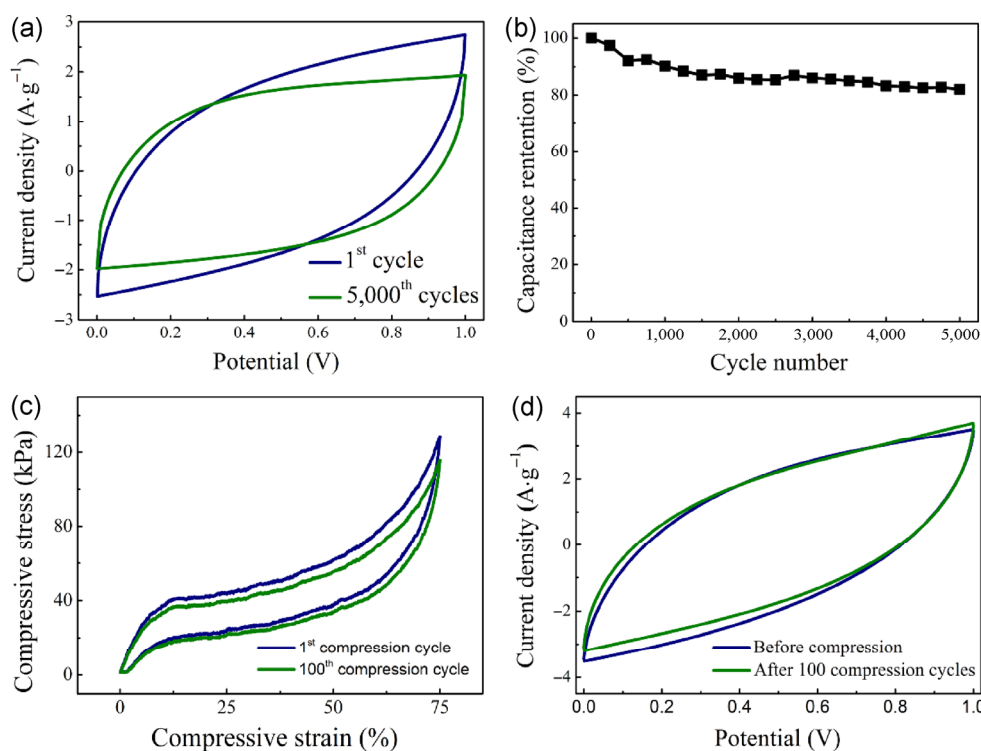


**Figure 6** Cycling stabilities of the MF-G-PPy-2 electrodes. (a) CV curves of the MF-G-PPy-2 electrode at 1 and 5,000 cycles. (b) Capacitance retention of the MF-G-PPy-2 electrode during 5,000 cycles. (c) Typical compression stress–strain curves of MF-G-PPy-2 at 1 and 100 compression cycles. (d) CV curves of the MF-G-PPy-2 electrode before compression and after 100 compression–release cycles at a compressive strain of 75%.

cycles. The electrode maintained its structural integrity, with almost no more broken skeletons after cycles (Fig. S4(a) in the ESM), indicating that the excellent cycling performance for the MF-G-PPy-2 electrode is possibly attributed to the unique 3D porous network, providing shorter path lengths for the transport of ions and better accommodation of the strain attributed to the electrochemical process. Meanwhile, the high-magnification SEM image of the MF-G-PPy-2 electrode after cycles (Fig. S4(b) in the ESM) indicated that a well-defined core–double-shell configuration of the MF-G-PPy electrode is maintained, and only marginal aggregation of PPy particles occurs after repeated charge–discharge cycles. Furthermore, cross-sectional SEM image of the MF-G-PPy-2 electrode after 5,000 charge–discharge cycles (Fig. S4(c) in the ESM) also confirms that strong adhesion between graphene and PPy layers occurs even after long time cycles. The above results demonstrate that the 3D interconnected porous structure designed here is extremely stable with excellent cycling performance. Furthermore, the mechanical properties of the as-prepared MF-G-PPy-2 electrodes were assessed by the measurement of the compressive stress–strain curves. Figure 6(c) shows the typical stress–strain curves of the MF-G-PPy-2 sample at compression–release cycles of 1 and 100. During repeated compressions at a compressive strain of 75%, the electrode material recovered its initial shape and maintained a similar compressive stress (ca. 115 kPa) with marginal degradation of mechanical strength (Fig. 6(c)). Plastic deformation was measured to be less than 3% as compared with the initial shape after 100 compression–release cycles up to a compressive strain of 75%, indicating that the MF-G-PPy-2 sample maintains superelasticity under repeated compression conditions. As shown in Fig. 6(d), after 100 compression–release cycles, the CV curve for the MF-G-PPy-2 electrode indicated that its electrochemical performance is not altered after repeated compression–release cycles. Notably, Fig. S5 in the ESM shows the large-scale fabrication of the MF-G-PPy-2 electrode, indicating that facile scale-up is possible for the production of 3D sponge electrodes with excellent deformation-tolerant performances.

## 4 Conclusions

In summary, we develop a simple, efficient route for fabricating a high-deformation-tolerant electrode by constructing two alternating layers (graphene layer and PPy layer in sequence) on commercial MFs via conventional LBL assembly and *in situ* polymerization. The resultant ternary MF-G-PPy composite sponges not only afford precise control over hierarchical structures with interconnected networks but also exhibit an excellent deformation-tolerant ability and good cycling stability during long-term charge–discharge. We observe that such an MF-G-PPy electrode exhibits an excellent gravimetric capacitance of  $427 \text{ F}\cdot\text{g}^{-1}$ ; this value is superior to those observed for other compressible electrode materials reported thus far, and it maintains its capacitance up to 92.1% at a compressive strain of 50%. The synergistic effect of the rationally designed graphene/PPy double-shell structure results in enhanced charging–discharging performance with a capacitance retention of 82% after 5,000 cycles. Furthermore, the electrochemical performance of the MF-G-PPy electrode is almost not altered after 100 repeated compression–release cycles. This study highlights the manner in which highly ordered 3D graphene structures and deformation-tolerant electrode materials can be simply constructed using commercial polymer foams.

## Acknowledgements

The authors gratefully acknowledge the National Natural Science Foundation of China (No. 21504012, 51125011 and 51433001) and the Fundamental Research Funds for the Central Universities of China (No. 16D110617).

**Electronic Supplementary Material:** Supplementary material (Raman spectra of the MF-GO and MF-G, SEM images of MF-G-10, CV curves of MF-G-PPy, upscaled fabrication of deformation-tolerant electrode materials in a big size, performance comparison of compressible electrodes) is available in the online version of this article at <http://dx.doi.org/10.1007/s12274-016-1179-6>.

## References

- [1] Xiao, X.; Ding, T. P.; Yuan, L. Y.; Shen, Y. Q.; Zhong, Q. Z.; Zhang, X. H.; Cao, Y. Z.; Hu, B.; Zhai, T.; Gong, L. et al. WO<sub>3-x</sub>/MoO<sub>3-x</sub> core/shell nanowires on carbon fabric as an anode for all-solid-state asymmetric supercapacitors. *Adv. Energy Mater.* **2012**, *2*, 1328–1332.
- [2] Lu, X. H.; Yu, M. H.; Zhai, T.; Wang, G. M.; Xie, S. L.; Liu, T. Y.; Liang, C. L.; Tong, Y. X.; Li, Y. High energy density asymmetric quasi-solid-state supercapacitor based on porous vanadium nitride nanowire anode. *Nano Lett.* **2013**, *13*, 2628–2633.
- [3] Lu, Q.; Chen, J. G.; Xiao, J. Q. Nanostructured electrodes for high-performance pseudocapacitors. *Angew. Chem., Int. Ed.* **2013**, *52*, 1882–1889.
- [4] Zhang, G. Q.; Lou, X. W. D. General solution growth of mesoporous NiCo<sub>2</sub>O<sub>4</sub> nanosheets on various conductive substrates as high-performance electrodes for supercapacitors. *Adv. Mater.* **2013**, *25*, 976–979.
- [5] Lu, X. H.; Yu, M. H.; Wang, G. M.; Zhai, T.; Xie, S. L.; Ling, Y. C.; Tong, Y. X.; Li, Y. H-TiO<sub>2</sub>@MnO<sub>2</sub>/h-TiO<sub>2</sub>@C core-shell nanowires for high performance and flexible asymmetric supercapacitors. *Adv. Mater.* **2013**, *25*, 267–272.
- [6] Chen, P. C.; Shen, G. Z.; Shi, Y.; Chen, H. T.; Zhou, C. W. Preparation and characterization of flexible asymmetric supercapacitors based on transition-metal-oxide nanowire/single-walled carbon nanotube hybrid thin-film electrodes. *ACS Nano* **2010**, *4*, 4403–4411.
- [7] Guan, C.; Xia, X. H.; Meng, N.; Zeng, Z. Y.; Cao, X. H.; Soci, C.; Zhang, H.; Fan, H. J. Hollow core-shell nanostructure supercapacitor electrodes: Gap matters. *Energy Environ. Sci.* **2012**, *5*, 9085–9090.
- [8] Xia, X. H.; Zhu, C. R.; Luo, J. S.; Zeng, Z. Y.; Guan, C.; Ng, C. F.; Zhang, H.; Fan, H. J. Synthesis of free-standing metal sulfide nanoarrays via anion exchange reaction and their electrochemical energy storage application. *Small* **2014**, *10*, 766–773.
- [9] Zhang, F.; Yuan, C. Z.; Zhu, J. J.; Wang, J.; Zhang, X. G.; Lou, X. W. D. Flexible films derived from electrospun carbon nanofibers incorporated with Co<sub>3</sub>O<sub>4</sub> hollow nanoparticles as self-supported electrodes for electrochemical capacitors. *Adv. Funct. Mater.* **2013**, *23*, 3909–3915.
- [10] Zhu, J. X.; Zhu, T.; Zhou, X. Z.; Zhang, Y. Y.; Lou, X. W.; Chen, X. D.; Zhang, H.; Hng, H. H.; Yan, Q. Y. Facile synthesis of metal oxide/reduced graphene oxide hybrids with high lithium storage capacity and stable cyclability. *Nanoscale* **2011**, *3*, 1084–1089.
- [11] Liu, J. L.; Zhang, L. L.; Wu, H. B.; Lin, J. Y.; Shen, Z. X.; Lou, X. W. D. High-performance flexible asymmetric supercapacitors based on a new graphene foam/carbon nanotube hybrid film. *Energy Environ. Sci.* **2014**, *7*, 3709–3719.
- [12] Cao, X. H.; Yin, Z. Y.; Zhang, H. Three-dimensional graphene materials: Preparation, structures and application in supercapacitors. *Energy Environ. Sci.* **2014**, *7*, 1850–1865.
- [13] Wang, G. K.; Sun, X.; Lu, F. Y.; Sun, H. T.; Yu, M. P.; Jiang, W. L.; Liu, C. S.; Lian, J. Flexible pillared graphene-paper electrodes for high-performance electrochemical supercapacitors. *Small* **2012**, *8*, 452–459.
- [14] Luo, B.; Liu, S.; Zhi, L. Chemical approaches toward graphene-based nanomaterials and their applications in energy-related areas. *Small* **2012**, *8*, 630–646.
- [15] Yin, S. Y.; Niu, Z. Q.; Chen, X. D. Assembly of graphene sheets into 3D macroscopic structures. *Small* **2012**, *8*, 2458–2463.
- [16] Wang, X. F.; Liu, B.; Liu, R.; Wang, Q. F.; Hou, X. J.; Chen, D.; Wang, R. M.; Shen, G. Z. Fiber-based flexible all-solid-state asymmetric supercapacitors for integrated photodetecting system. *Angew. Chem., Int. Ed.* **2014**, *126*, 1880–1884.
- [17] Wang, X. F.; Lu, X. H.; Liu, B.; Chen, D.; Tong, Y. X.; Shen, G. Z. Flexible energy-storage devices: Design consideration and recent progress. *Adv. Mater.* **2014**, *26*, 4763–4782.
- [18] Luo, B.; Zhi, L. J. Design and construction of three dimensional graphene-based composites for lithium ion battery applications. *Energy Environ. Sci.* **2015**, *8*, 456–477.
- [19] Chen, T.; Wang, S. T.; Yang, Z. B.; Feng, Q. Y.; Sun, X. M.; Li, L.; Wang, Z. S.; Peng, H. S. Flexible, light-weight, ultrastrong, and semiconductive carbon nanotube fibers for a highly efficient solar cell. *Angew. Chem., Int. Ed.* **2011**, *50*, 1815–1819.
- [20] Ren, J.; Bai, W. Y.; Guan, G. Z.; Zhang, Y.; Peng, H. S. Flexible and weaveable capacitor wire based on a carbon nanocomposite fiber. *Adv. Mater.* **2013**, *25*, 5965–5970.
- [21] Cong, H.-P.; Ren, X.-C.; Wang, P.; Yu, S.-H. Flexible graphene-polyaniline composite paper for high-performance supercapacitor. *Energy Environ. Sci.* **2013**, *6*, 1185–1191.
- [22] He, Y. M.; Chen, W. J.; Li, X. D.; Zhang, Z. X.; Fu, J. C.; Zhao, C. H.; Xie, E. Q. Freestanding three-dimensional graphene/MnO<sub>2</sub> composite networks as ultralight and flexible supercapacitor electrodes. *ACS Nano* **2013**, *7*, 174–182.
- [23] Chen, L.-F.; Huang, Z.-H.; Liang, H.-W.; Yao, W.-T.; Yu, Z.-Y.; Yu, S.-H. Flexible all-solid-state high-power supercapacitor fabricated with nitrogen-doped carbon nanofiber electrode material derived from bacterial cellulose. *Energy Environ. Sci.* **2013**, *6*, 3331–3338.

- [24] Wang, Q.; Yan, J.; Fan, Z. Q. Carbon materials for high volumetric performance supercapacitors: Design, progress, challenges and opportunities. *Energy Environ. Sci.* **2016**, *9*, 729–762.
- [25] Dimesso, L.; Spanheimer, C.; Jacke, S.; Jaegermann, W. Synthesis and characterization of three-dimensional carbon foams-LiFePO<sub>4</sub> composites. *J. Power Sources* **2011**, *196*, 6729–6734.
- [26] Kodama, M.; Yamashita, J.; Soneda, Y.; Hatori, H.; Kamegawa, K. Preparation and electrochemical characteristics of N-enriched carbon foam. *Carbon* **2007**, *45*, 1105–1107.
- [27] Chen, S. L.; Liu, Q.; He, G. H.; Zhou, Y.; Hanif, M.; Peng, X. W.; Wang, S. Q.; Hou, H. Q. Reticulated carbon foam derived from a sponge-like natural product as a high-performance anode in microbial fuel cells. *J. Mater. Chem.* **2012**, *22*, 18609–18613.
- [28] Zhao, Y.; Liu, J.; Hu, Y.; Cheng, H. H.; Hu, C. G.; Jiang, C. C.; Jiang, L.; Cao, A. Y.; Qu, L. T. Highly compression-tolerant supercapacitor based on polypyrrole-mediated graphene foam electrodes. *Adv. Mater.* **2013**, *25*, 591–595.
- [29] Li, X.; Rong, J. P.; Wei, B. Q. Electrochemical behavior of single-walled carbon nanotube supercapacitors under compressive stress. *ACS Nano* **2010**, *4*, 6039–6049.
- [30] Li, P. X.; Kong, C. Y.; Shang, Y. Y.; Shi, E. Z.; Yu, Y. T.; Qian, W. Z.; Wei, F.; Wei, J. Q.; Wang, K. L.; Zhu, H. W. et al. Highly deformation-tolerant carbon nanotube sponges as supercapacitor electrodes. *Nanoscale* **2013**, *5*, 8472–8479.
- [31] Li, P. X.; Shi, E. Z.; Yang, Y. B.; Shang, Y. Y.; Peng, Q. Y.; Wu, S. T.; Wei, J. Q.; Wang, K. L.; Zhu, H. W.; Yuan, Q. et al. Carbon nanotube-polypyrrole core-shell sponge and its application as highly compressible supercapacitor electrode. *Nano Res.* **2014**, *7*, 209–218.
- [32] Cao, X. H.; Shi, Y. M.; Shi, W. H.; Lu, G.; Huang, X.; Yan, Q. Y.; Zhang, Q. C.; Zhang, H. Preparation of novel 3D graphene networks for supercapacitor applications. *Small* **2011**, *7*, 3163–3168.
- [33] Chen, S. L.; He, G. H.; Hu, H.; Jin, S. Q.; Zhou, Y.; He, Y. Y.; He, S. J.; Zhao, F.; Hou, H. Q. Elastic carbon foam via direct carbonization of polymer foam for flexible electrodes and organic chemical absorption. *Energy Environ. Sci.* **2013**, *6*, 2435–2439.
- [34] He, S. J.; Chen, W. High performance supercapacitors based on three-dimensional ultralight flexible manganese oxide nanosheets/carbon foam composites. *J. Power Sources* **2014**, *262*, 391–400.
- [35] Zhu, G. X.; Xi, C. Y.; Liu, Y. J.; Zhu, J.; Shen, X. P. CN foam loaded with few-layer graphene nanosheets for high-performance supercapacitor electrodes. *J. Mater. Chem. A* **2015**, *3*, 7591–7599.
- [36] Fan, Z. J.; Yan, J.; Zhi, L. J.; Zhang, Q.; Wei, T.; Feng, J.; Zhang, M. L.; Qian, W. Z.; Wei, F. A three-dimensional carbon nanotube/graphene sandwich and its application as electrode in supercapacitors. *Adv. Mater.* **2010**, *22*, 3723–3728.
- [37] Gui, X. C.; Wei, J. Q.; Wang, K. L.; Cao, A. Y.; Zhu, H. W.; Jia, Y.; Shu, Q. K.; Wu, D. H. Carbon nanotube sponges. *Adv. Mater.* **2010**, *22*, 617–621.
- [38] Basiricò, L.; Lanzara, G. Moving towards high-power, high-frequency and low-resistance cnt supercapacitors by tuning the cnt length, axial deformation and contact resistance. *Nanotechnology* **2012**, *23*, 305401.
- [39] Li, P. X.; Yang, Y. B.; Shi, E. Z.; Shen, Q. C.; Shang, Y. Y.; Wu, S. T.; Wei, J. Q.; Wang, K. L.; Zhu, H. W.; Yuan, Q. et al. Core-double-shell, carbon nanotube@polypyrrole@MnO<sub>2</sub> sponge as freestanding, compressible supercapacitor electrode. *ACS Appl. Mater. Interfaces* **2014**, *6*, 5228–5234.
- [40] Liang, H. W.; Guan, Q. F.; Chen, L. F.; Zhu, Z.; Zhang, W. J.; Yu, S. H. Macroscopic-scale template synthesis of robust carbonaceous nanofiber hydrogels and aerogels and their applications. *Angew. Chem., Int. Ed.* **2012**, *51*, 5101–5105.
- [41] Hu, H.; Zhao, Z. B.; Wan, W. B.; Gogotsi, Y.; Qiu, J. S. Ultralight and highly compressible graphene aerogels. *Adv. Mater.* **2013**, *25*, 2219–2223.
- [42] Huang, X.; Yin, Z. Y.; Wu, S. X.; Qi, X. Y.; He, Q. Y.; Zhang, Q. C.; Yan, Q. Y.; Boey, F.; Zhang, H. Graphene-based materials: Synthesis, characterization, properties, and applications. *Small* **2011**, *7*, 1876–1902.
- [43] Tao, Y.; Xie, X. Y.; Lv, W.; Tang, D.-M.; Kong, D. B.; Huang, Z. H.; Nishihara, H.; Ishii, T.; Li, B. H.; Golberg, D. et al. Towards ultrahigh volumetric capacitance: Graphene derived highly dense but porous carbons for supercapacitors. *Sci. Rep.* **2013**, *3*, 2975.
- [44] Hu, Y.; Cheng, H. H.; Zhao, F.; Chen, N.; Jiang, L.; Feng, Z. H.; Qu, L. T. All-in-one graphene fiber supercapacitor. *Nanoscale* **2014**, *6*, 6448–6451.
- [45] Lu, X. H.; Zhai, T.; Zhang, X. H.; Shen, Y. Q.; Yuan, L. Y.; Hu, B.; Gong, L.; Chen, J.; Gao, Y. H.; Zhou, J. et al. WO<sub>3-x</sub>@Au@MnO<sub>2</sub> core-shell nanowires on carbon fabric for high-performance flexible supercapacitors. *Adv. Mater.* **2012**, *24*, 938–944.
- [46] Niu, Z. Q.; Zhou, W. Y.; Chen, X. D.; Chen, J.; Xie, S. S. Highly compressible and all-solid-state supercapacitors based on nanostructured composite sponge. *Adv. Mater.* **2015**, *27*, 6002–6008.
- [47] Niu, Z. Q.; Dong, H. B.; Zhu, B. W.; Li, J. Z.; Hng, H. H.; Zhou, W. Y.; Chen, X. D.; Xie, S. S. Highly stretchable,

- integrated supercapacitors based on single-walled carbon nanotube films with continuous reticulate architecture. *Adv. Mater.* **2013**, *25*, 1058–1064.
- [48] Wu, X. L.; Yang, D. R.; Wang, C. K.; Jiang, Y. T.; Wei, T.; Fan, Z. J. Functionalized three-dimensional graphene networks for high performance supercapacitors. *Carbon* **2015**, *92*, 26–30.
- [49] Marcano, D. C.; Kosynkin, D. V.; Berlin, J. M.; Sinitskii, A.; Sun, Z. Z.; Slesarev, A.; Alemany, L. B.; Lu, W.; Tour, J. M. Improved synthesis of graphene oxide. *ACS Nano* **2010**, *4*, 4806–4814.
- [50] Li, Z. P.; Wang, J. Q.; Liu, X. H.; Liu, S.; Ou, J. F.; Yang, S. R. Electrostatic layer-by-layer self-assembly multilayer films based on graphene and manganese dioxide sheets as novel electrode materials for supercapacitors. *J. Mater. Chem.* **2011**, *21*, 3397–3403.
- [51] Sheng, K. X.; Bai, H.; Sun, Y. Q.; Li, C.; Shi, G. Q. Layer-by-layer assembly of graphene/polyaniline multilayer films and their application for electrochromic devices. *Polymer* **2011**, *52*, 5567–5572.
- [52] Lee, T.; Yun, T.; Park, B.; Sharma, B.; Song, H.-K.; Kim, B.-S. Hybrid multilayer thin film supercapacitor of graphene nanosheets with polyaniline: Importance of establishing intimate electronic contact through nanoscale blending. *J. Mater. Chem.* **2012**, *22*, 21092–21099.